Chemistry–A European Journal

Full Paper
doi.org/10.1002/chem.202102377

Chemistry
Europe
European Chemical
Societies Publishing

A Molecular Photosensitizer in a Porous Block Copolymer Matrix-Implications for the Design of Photocatalytically Active Membranes

Avinash Chettri,[a, b] Jan-Hendrik Kruse,[c] Keshav Kumar Jha,[a, b] Lara Dröge,[a, b] Iuliia Romanenko,[c] Christof Neumann,[b] Stephan Kupfer,[b] Andrey Turchanin,[b, e] Sven Rau,[d] Felix H. Schacher,[c, e] and Benjamin Dietzek*[a, b]

Abstract: Recently, porous photocatalytically active block copolymer membranes were introduced, based on heterogenized molecular catalysts. Here, we report the integration of the photosensitizer, i.e., the light absorbing unit in an intermolecular photocatalytic system into block copolymer membranes in a covalent manner. We study the resulting structure and evaluate the orientational mobility of the photosensitizer as integral part of the photocatalytic system in such membranes. To this end we utilize transient absorption anisotropy, highlighting the temporal reorienta- tion of the transition dipole moment probed in a femto- second pump-probe experiment. Our findings indicate that the photosensitizer is rigidly bound to the polymer mem- brane and shows a large heterogeneity of absolute anisotropy values as a function of location probed within the matrix. This reflects the sample inhomogeneity arising from different protonation states of the photosensitizer and different intermolecular interactions of the photosensitizers within the block copolymer membrane scaffold.

Introduction

Nanoporous block copolymer membranes, which are typically formed by self-assembly processes, are versatile platforms that can be used for a variety of applications, for example, in flow reactors, for catalysis, for water purification, or protein separation.[1–5] Hereby, the underlying amphiphilic block copoly- mers can be adapted for different purposes, may contain a large variety of functional groups, and have large impact on the properties of the resulting membranes. The tuning of mem- brane properties can primarily be conducted by the application of different monomers and variation of the ratio of the share of hydrophilic and hydrophobic block. This is an advantage in comparison to classical inorganic supports, which in some cases may be more stable but are usually far less adaptable.[6,7]

Depending on the desired application such block copolymer membranes can also be functionalized with different com- pounds to impart specific properties.[8] One example are membranes for catalytic processes in which catalysts are immobilized on the surface of a membrane. Such systems, in which heterogenized molecular catalysts are integrated into nanostructured soft matter matrices, are interesting for future applications in energy conversion technologies. For this immobilization different mechanisms are possible. The simplest method is an electrostatic attachment, that is realized by opposite charges of catalyst and membrane surface.[1,8] Another option is covalent immobilization. This increases the stability of the connection between functional unit and membrane but requires the introduction of a suitable combination of func- tional groups into both underlying block copolymer and catalyst.

Depending on the kind of targeted catalysis, it can also be necessary to introduce further compounds, for example, photo- sensitizers which again can be introduced electrostatically or by covalent interactions. However, as an additional prerequisite a certain proximity is necessary between catalyst and photo-

[a] A. Chettri, K. Kumar Jha, L. Dröge, Prof. Dr. B. Dietzek
Department Functional Interfaces
Leibniz Institute of Photonic Technology (IPHT) e.V.
Albert Einstein Straße 9, 07747 Jena (Germany)
E-mail: benjamin.dietzek@leibniz-ipht.de

[b] A. Chettri, K. Kumar Jha, L. Dröge, Dr. C. Neumann, Dr. S. Kupfer,
Prof. Dr. A. Turchanin, Prof. Dr. B. Dietzek
Institute of Physical Chemistry
Friedrich Schiller University Jena
Helmholtzweg 4, 07743 Jena (Germany)

[c] J.-H. Kruse, Dr. I. Romanenko, Prof. Dr. F. H. Schacher
Institute of Organic Chemistry and Macromolecular Chemistry
Friedrich Schiller University Jena
Lessingstraße 8, 07743 Jena (Germany)

[d] Prof. Dr. S. Rau
Institute of Inorganic Chemistry I
Ulm University
Albert Einstein Allee 11, 89081 Ulm (Germany)

[e] Prof. Dr. A. Turchanin, Prof. Dr. F. H. Schacher
Jena Center for Soft Matter (JCSM)
Philosophenweg 7, 07743 Jena (Germany)

Supporting information for this article is available on the WWW under https://doi.org/10.1002/chem.202102377

Part of a Special Issue on Contemporary Challenges in Catalysis.

Chemistry–A European Journal

Full Paper
doi.org/10.1002/chem.202102377

**Chemistry
Europe**
European Chemical
Societies Publishing

sensitizer to ensure an efficient energy transfer. In an earlier example, a positively charged Ru(bpy)₃ (bpy = 2,2′-bipyridine) photosensitizer was attached to a nanoporous block copolymer membrane by electrostatic interactions with a previously immobilized and negatively charged molybdenum sulfide catalyst. This combination led to successful light-driven hydrogen evolution reaction (HER).[9] In other examples, ruthenium-based photosensitizers were also introduced covalently to different polymers for electro-optical applications. This allows a more stable functionalization and an increased amount of photosensitizer in the polymer in comparison to electrostatic functionalization. However, these polymers were not yet used in membranes.[10–12]

Herein, we demonstrate an alternative approach for the covalent functionalization of a nanoporous block copolymer membrane with a ruthenium-based photosensitizer, which also leads to an increased amount of photosensitizer in the membrane compared to the electrostatic attachment approach that we reported before.[9]

Immobilizing photosensitizers on substrates often causes challenges to be met, which are not relevant when studying the photosensitizers in homogeneous solution. Prime examples for such challenges are the formation of aggregates between individual molecular sensitizers in dye-sensitized solar cells (DSSC)[13,14] or accelerated excited-state decay in DSSC[15] or dye-sensitized photoelectrochemical cells due to self-quenching of the optically excited dyes.[16,17] More specifically, when incorporating concepts of molecular photocatalysis into membranes by immobilization of individual components of a photocatalytically active system, not only reactant and product transport to and from the inner walls of the photocatalytically active membrane will impact the photocatalytic reaction but also the ability of the immobilized reaction partners to partake in the intermolecular collisions, which are inherent to the overall photocatalytic mechanism.

This contribution particularly focusses on the latter aspect, which - to the best of our knowledge - has not yet been explored experimentally. To this end, we study the transient absorption anisotropy of a Ru photosensitizer, the chloride salt of [**Ru(bpy)₂(ipPhNH₂)**]²⁺ (bpy = 2,2′-bipyridine, ipPhNH₂ = 2-[4-phenylamino]-1H-imidazo[4,5-f][1,10]phenanthroline), which is linked to a porous block copolymer membrane (from here on referred to as Ru-membranes) as introduced below (Figure 1) We use a diblock copolymer with a hydrophobic block consisting of a poly(styrene-co-isoprene) copolymer (P(S-co-I)) and a poly(tri(ethylene glycol) methyl ether acrylate)-co-(vinylbenzyl chloride) copolymer (P(TEGA-co-VBCl)) as hydrophilic segment. The VBCl units can then be utilized for the functionalization with the photosensitizer.

To put the results of the transient absorption anisotropy measurements into context, we complement these experiments with absorption, steady state and time-resolved emission and resonance Raman (rR) spectroscopy. The data presented highlights the importance of a detailed understanding of the changes in the photosensitizer environment upon material integration to the molecular system.

Results and Discussion

For the preparation of the Ru-membrane the diblock copolymer was synthesized in a two-step procedure. In the first step, the two hydrophobic monomers styrene and isoprene were copolymerized via nitroxide-mediated polymerization (NMP) to form poly(styrene-co-isoprene) P(S$_{78}$-co-I$_{22}$)^{38} (M_n = 37,800 g mol⁻¹, Đ = 1.25, determined via size-exclusion chromatography (SEC, Figure S1))-the subscripts denote the respective weight fraction in % and the superscript the overall molar mass in kg/mol. This block later forms the membrane scaffold, the isoprene units increase the flexibility of the material and due to their leftover
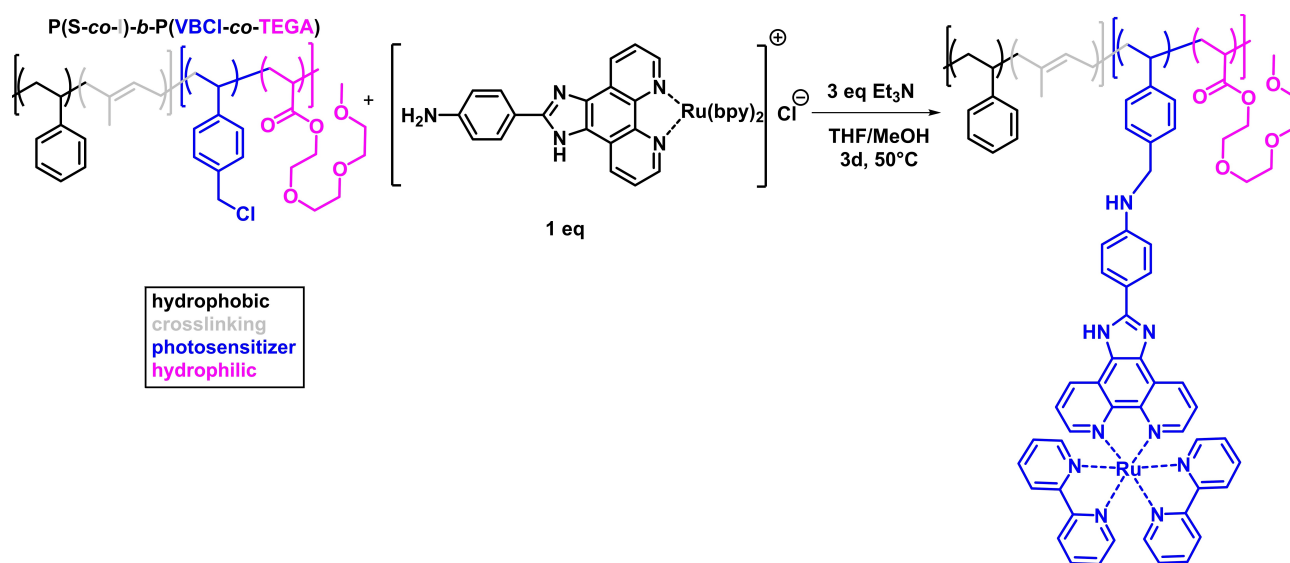

Figure 1. Functionalization of the **P(S$_{39}$-co-I$_{11}$)-b-P(TEGA$_{14}$-co-VBCl$_{36}$)^{75}** diblock copolymer with [**Ru(bpy)₂(ipPhNH₂)**]²⁺ photosensitizer. The chlorine atom of the VBCl unit reacts in a nucleophilic substitution with the amine of the photosensitizer.

Chemistry–A European Journal

Full Paper
doi.org/10.1002/chem.202102377

Chemistry Europe
European Chemical
Societies Publishing

double bond after the polymerization could also be used for crosslinking of different polymer strains to increase stability.

In the second step this copolymer was used as macro-initiator for the NMP copolymerization of TEGA and VBCl which led to the final diblock tetrapolymer P(S$_{39}$-co-I$_{11}$)-b-P(TEGA$_{14}$-co-VBCl$_{36}$)^{75} (M$_n$ = 74,600 g mol^{-1}, Đ = 1.37, determined via nuclear magnetic resonance (NMR) spectroscopy (Figure S2)). This block has a higher polarity than the first block due to the TEGA units. The VBCl units can be utilized for the covalent functionalization with [Ru(bpy)$_2$(ipPhNH$_2$)]$^{2+}$ (ipPhNH$_2$ = 2-[4-phenlyamino]-1H-imidazo[4,5-f][1,10]phenanthr-oline) photosensitizers. A higher share of VBCl in the hydrophilic block would reduce the sterical hindrance and increase the number of possible anchoring sites for the photosensitizer but also decrease the hydrophilicity and, with that, would influence the membrane formation process.

From these diblock copolymers the membranes were formed via the non-solvent induced phase separation (NIPS) process (Figure 2). Different open times and ratios of solvents for the NIPS process were tested. A mixture of tetrahydrofuran (THF) and dimethylformamide (DMF) (70/30 wt%) and an open time of 15 s provided membranes with an appropriate morphology and porosity.

The membranes were afterwards analyzed by SEM (Figures 3b and c). In the cross-section of the Ru-membrane a finger-like morphology of the pores can be observed in combination with sponge-like pores between the larger finger-like structures, the membrane thickness is about 52 μm. On both sides of the Ru-membrane, surface pores with a diameter of about 0.1–1 μm can be observed. The pore distribution is not regular, but the pores are distributed over the whole surface and allow water flux through the membrane.

After the membrane formation the functionalization with the [Ru(bpy)$_2$(ipPhNH$_2$)]$^{2+}$ photosensitizer was carried out. This photosensitizer features an amine group at the ipPhNH$_2$ ligand that can be covalently linked to the VBCl comonomers in the hydrophilic block by a nucleophilic substitution at the chlorine atom, leading to the functionalized Ru-membrane (Figure 2).

The hydrophobic block of the block copolymers forms the membrane scaffold while the hydrophilic block mainly is located at the pore surface of the membrane due to the self-assembly process during the membrane formation.[7,24] Therefore, the hydrophilic block is accessible for functionalization with the photosensitizer, which leads to permanent linkage of the photosensitizer to the polymer backbone (Figure 2).
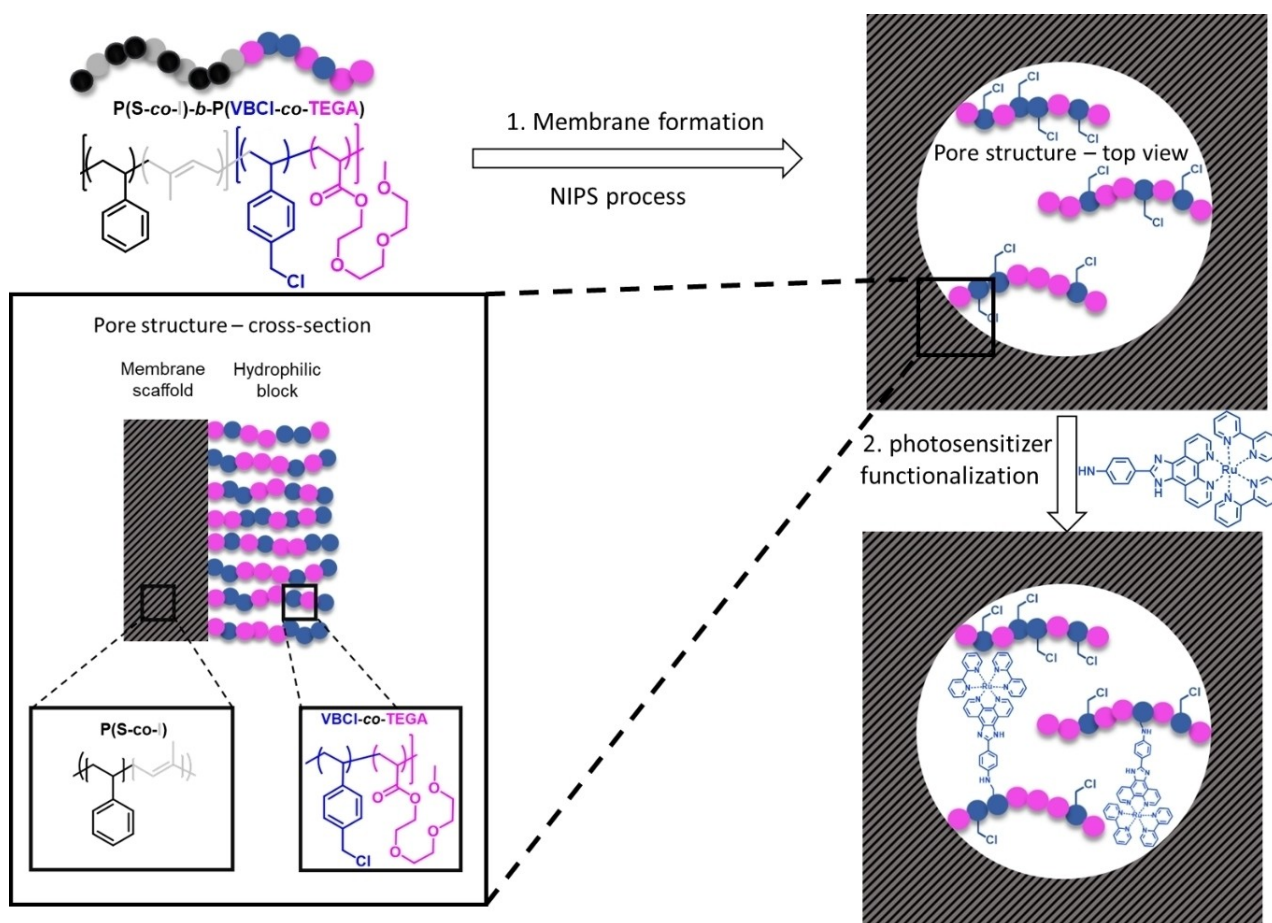

Figure 2. Schematic overview of the Ru-membrane formation and the membrane structure before and after the functionalization with the [Ru(bpy)$_2$(ipPhNH$_2$)]$^{2+}$ photosensitizer.
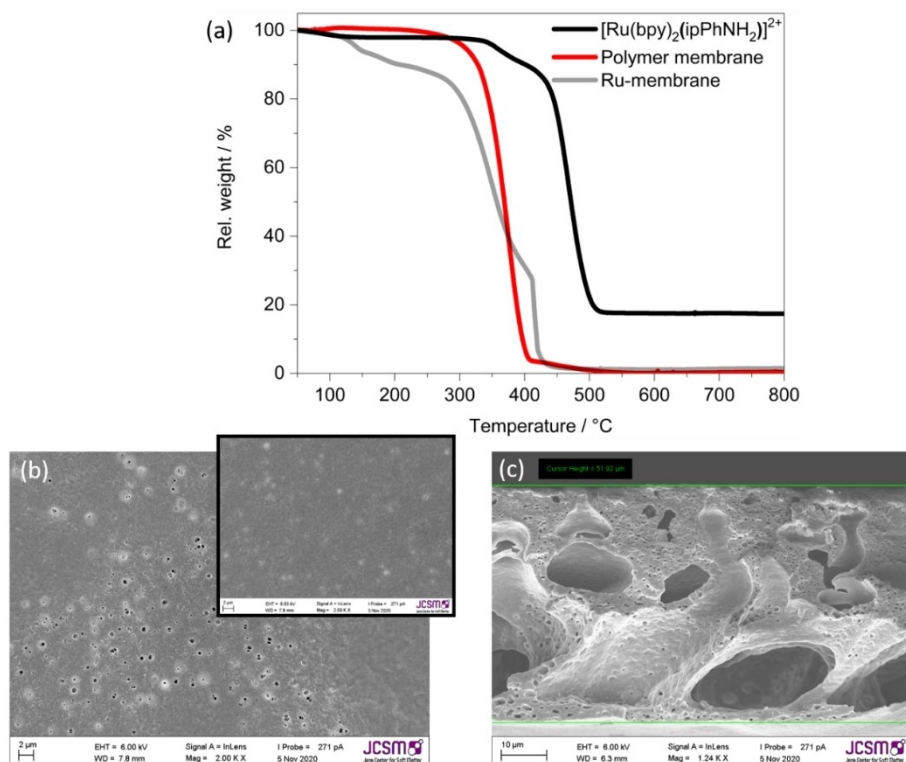
Chemistry–A European Journal

Full Paper
doi.org/10.1002/chem.202102377

Chemistry Europe
European Chemical
Societies Publishing

Figure 3. (a) Thermogravimetric analysis (TGA) graph of the Ru-membrane after functionalization and the pure [**Ru(bpy)$_2$(ipPhNH$_2$)**]$^{2+}$ photosensitizer, according to this data the photosensitizer has a weight share of 6.5 wt% of the membrane; Scanning electron microscopy (SEM) micrographs of the Ru-membrane before functionalization. (b) Top view of both sides. (c) Cross-section.

The degree of functionalization was analyzed via thermogravimetric analysis (TGA) which showed that the weight share of the photosensitizer was 6.5 wt% of the membrane. This corresponds to a degree of functionalization of about 3.9% of all available VBCl units. This accuracy in our opinion is sufficient at this point to (repeatedly) prove the presence of significant amounts of the photosensitizer within the membrane pores. The successful functionalization of the membrane with the photosensitizer was additionally proven via X-ray photoelectron spectroscopy (XPS) (Figure S3). With this technique the elemental composition of the membrane surface can be analyzed. The analysis shows a molar fraction of ruthenium of 0.1 at% on the membrane surface (Table S1), which corresponds to a weight share of 0.75 wt%, and to approximately 5.4 wt% of the entire photosensitizer. This value is slightly lower than the weight share calculated via TGA measurements but the difference can be rather ascribed to the measurement error of the TGA. Additionally, only the surface of the membrane can be analyzed by XPS and only a small share of the pore surface is located on the surface of the membrane. Therefore, the difference between these numbers is in the expected range. Most importantly, the XPS measurements show the successful functionalization with the photosensitizer both via the presence of the Ru 3d$_{5/2}$ signal as well as by the modified shoulder of the C 1s peak due to additional –C–N bonds (see Supporting Information for details).

Overall, the rather low amount of photosensitizer can be explained by the large sterical demand of the complex with its two bpy ligands, limited accessibility of the VBCl units as the TEGA comonomers are also sterically demanding, and the fact that not all VBCl units are actually exposed on the membrane surface.

The overall hydrophilicity of the P(TEGA-*co*-VBCl) block in comparison to the PS block ensures that the VBCl units still are directed into the pores of the membrane. This is also supported by subsequent spectroscopic analysis (see below). Due to the high share of VBCl units in the polymer the Ru-membranes are intensely and homogeneously orange-colored (Figure S4). The amount of the photosensitizer in the membrane is constant over time and there was no visible leaching of photosensitizer after exchanging the storage solution of the membrane three times.

Absorption, resonance Raman and emission spectroscopy

The UV-vis absorption spectra of [**Ru(bpy)$_2$(ipPhNH$_2$)**]$^{2+}$ in H$_2$O show the characteristic metal-to-ligand charge transfer (MLCT) absorption band between 400 and 550 nm (Figure 4a) and resembles the absorption of prototypical [Ru(bpy)$_3$]$^{2+}$-type complexes.[25,26] The resonance Raman spectra of [**Ru(bpy)$_2$(ipPhNH$_2$)**]$^{2+}$, when compared to reference spectra of the related complexes [Ru(bpy)$_3$]$^{2+}$ and [Ru(dmb)$_2$ip]$^{2+}$, reveal that the Franck-Condon point of absorption at around 400 nm is delocalized over all three ligands of the complex (Figure S5).[27]
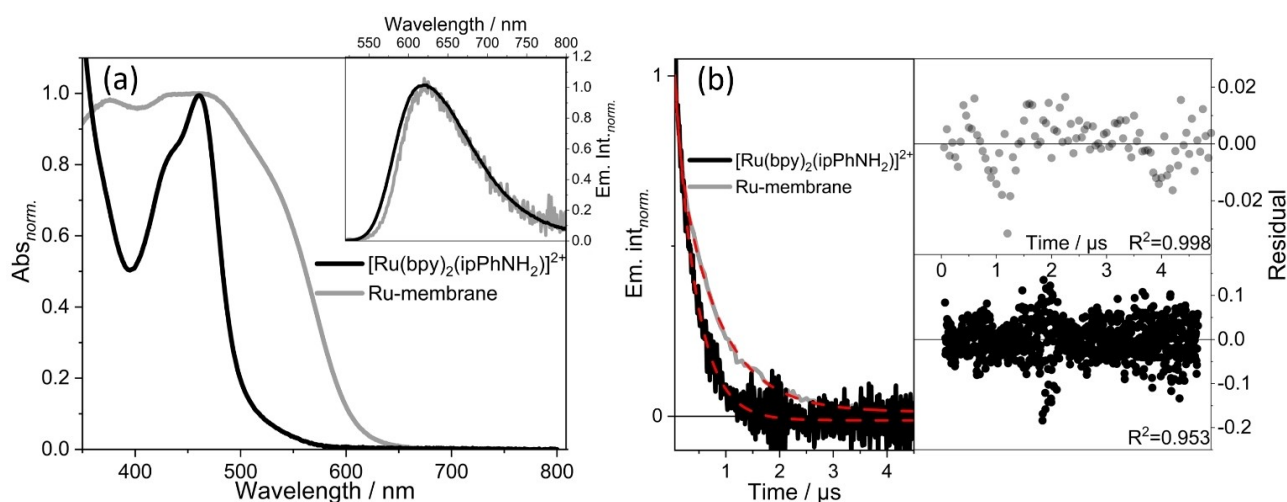
Chemistry–A European Journal

Full Paper
doi.org/10.1002/chem.202102377

Chemistry
Europe
European Chemical
Societies Publishing

Figure 4. (a) Steady state absorption of **[Ru(bpy)$_2$(ipPhNH$_2$)]$^{2+}$** and Ru-membrane with emission spectra in the inset at $\lambda_{ex.} = 410$ nm. (b) Time resolved emission kinetics recorded at $\lambda_{em.} = 620$ nm with $\lambda_{ex.} = 410$ nm in **[Ru(bpy)$_2$(ipPhNH$_2$)]$^{2+}$** in H$_2$O and Ru-membrane with their respective residual and R^2 obtained from the fits.

Integration of the complex into the polymer causes a red shift of the absorption maxima at 463 cm^{-1}. Simultaneously, the absorption band broadens above 550 nm (Figure 4a). This indicates that integration of the complexes into the polymer membrane introduces additional intermolecular interactions between the chromophores. Similar spectral shifts have been observed due to aggregation of a Ru[(bpy)$_3$]$^{2+}$-derived complex either in a spin coated PMMA film and on porous TiO$_2$ films.[28]

Monitoring the emission at 620 nm, a ^{3}MLCT lifetime of 350 ns was determined for **[Ru(bpy)$_2$(ipPhNH$_2$)]$^{2+}$** in H$_2$O (Figure 4b). Again this value is in good agreement with ^{3}MLCT lifetimes, for example, observed for [Ru(bpy)$_3$]$^{2+}$ and [Ru-(bpy)$_2$ip]$^{2+}$.[25,29] In the Ru-membrane, the emission signal decays bi-exponentially with lifetimes of 90 and 750 ns (Figure 4b). We assign the prolonged emission lifetime to the more rigid environment of the luminophore in the polymer membrane.[30,31] The short lifetime component, on the other hand, indicates self-quenching, which is quite common, for example, in dye-sensitized solar cells.[28,32–35] The bi-exponential emission decay hence indicates a non-uniform local environment of the complexes in the polymer membranes.

Femtosecond transient absorption and transient absorption anisotropy

Figure 5 displays the transient absorption data of **[Ru-(bpy)$_2$(ipPhNH$_2$)]$^{2+}$** dissolved in ACN (acetonitrile) and H$_2$O. The overall spectral signatures resemble the transient absorption data of [Ru(bpy)$_3$]$^{2+}$, [Ru(bpy)$_2$ip]$^{2+}$ and related complexes:[26,36,37] Upon excitation at 400 nm a ground-state bleach (GSB) centered at around 450 nm is accompanied by a sharp excited-state absorption (ESA) at ca. 350 nm and a broad, unstructured ESA band extending to the near-IR.[26] Since intersystem crossing (ISC) is generally fast in this type of complexes, i.e., sub-100 fs[38]

and hence within the limit of time-resolution in our setup, the earliest transient absorption spectrum reflects the properties of a triplet state. Here, the band at 350 nm is due to ligand-centered (LC) transitions of the reduced ligands,[25] while the ESA band extending to the red comprises both ligand-to-metal charge transfer (LMCT) and ipPhNH$_2$-centered transitions as predicted by quantum chemical simulations (Figure S8 and S9).[39]

The transient absorption data of the complex in solution are analyzed by a global fit of a multi-exponential function. To account for the differential absorption changes observed for **[Ru(bpy)$_2$(ipPhNH$_2$)]$^{2+}$** in ACN and H$_2$O a bi-exponential and tri-exponential model is required, respectively. The fit to the benchmark data of the complex in ACN solution yields two characteristic time constants, i.e., $\tau_1 = 0.5$ ps and $\tau_2 = 16$ ps. The presence of an infinite component implies a long-lived state being populated, which does not decay within the experimentally accessible delay time. This long-lived state is associated with a ^{3}MLCT state (see T$_1$ spin density in Figure S9), typically dominating the ns-photochemistry of this type of Ru-complexes. $\tau_1 = 1$ ps and $\tau_2 = 13$ ps reflect the formation of the long-lived state by intramolecular vibrational relaxation, cooling and thermalization of the ^{3}MLCT on the ip-ligand, which presents the ligand with the energetically lowest lying acceptor orbital.[39–42] When dissolved in H$_2$O an additional decay component, characterized by a decay constant of 645 ps, is observed. This decay component contributes to the decay of the red-extending ESA, while it essentially does not contribute to ground-state recovery. Thus, we ascribe the presence of this decay to a shift in the charge density from imidazole-phenanthroline to the aniline portion of the ligand (as shown, for example, by T$_{11}$ in Figure S9). This excited-state reaction step is favored by the presence of the protonated form of the aniline nitrogen. It is known that the pK$_a$ for deprotonation of the aniline group in a [Ru(bpy)$_2$ip]$^{2+}$-complex containing *N,N*-

Chemistry–A European Journal

Full Paper
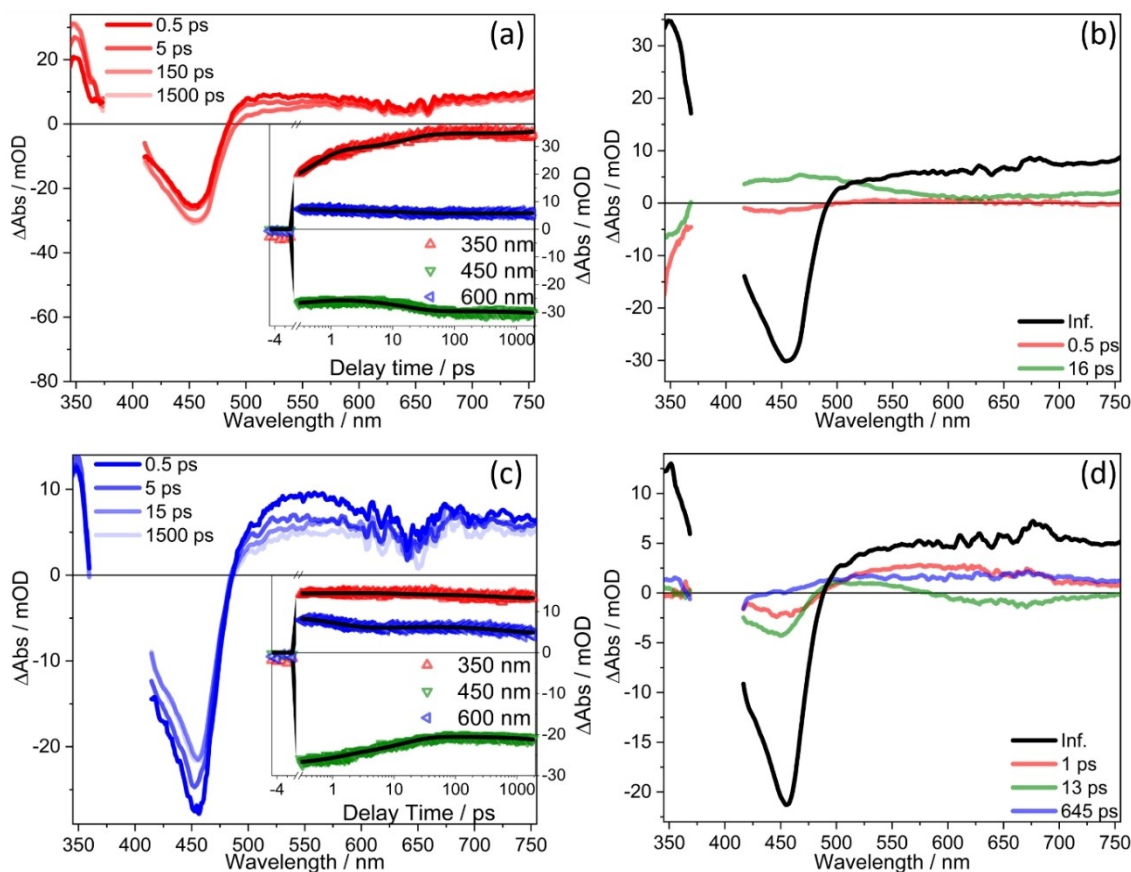doi.org/10.1002/chem.202102377

Chemistry
Europe
European Chemical
Societies Publishing

Figure 5. Benchmark transient absorption experiments of $[Ru(bpy)_2(ipPhNH_2)]^{2+}$ in solution. The samples were excited by pulses centered at $\lambda_{ex.} = 400$ nm and the subsequent relaxation dynamics was observed upon dissolution of the complex in ACN (panels (a) and (b)) and in water (panels (c) and (d)). Panels (a) and (c) depict selected differential absorption spectra and kinetics (see insets), while panels (b) and (d) depict the decay-associated spectra resulting from a multi-exponential fit of the data.

Dimethylaniline is in the range of 4–5[43] whereas the first and second deprotonation constant of imidazole are below 2 and above 10 respectively.[43–46] Therefore a near neutral condition should permit a fraction of molecules to exist with an electron withdrawing anilinium ion fragment. Hence, when dissolved in water (or embedded in the water wetted polymer membranes) the equilibrium shifts towards the protonated form of the complex as compared to ACN as solvent. The charge density shift from the imidazole-phenanthroline centered ^{3}MLCT to an aniline-centered ^{3}MLCT in the protonated form of the complex is hence reflected in the 645 ps component.

When studying the ultrafast transient absorption kinetics in the Ru-membrane, we restrict ourselves to single-wavelength probe measurements to deal with the increased scattering of the inhomogeneous membranes: We excite the Ru-membrane at 400 nm and probe the overall population of the ^{3}MLCT manifold at 600 nm. The magic angle kinetics, reflecting the overall population kinetics, recorded for Ru-membrane looks quite different than the respective kinetics for the complex dissolved in water: An initial positive ΔAbs turns into a negative signal with a characteristic time constant of 530 ps (Figure 6a). We associate this change in sign of the ΔAbs signal, with the presence of the extended GSB signal in this spectral region,

when incorporating the complexes in the membranes. On the time constant of 530 ps a charge transfer from phen to the protonated imidazole-aniline fragment diminishes the ESA and hence, the extended GSB starts dominating the overall signal. The absence of a fast, sub-10 ps decay component in Ru-membrane indicates altered energy dissipation upon integration of the complex into the restricted molecular environment of the membrane. However, as we cannot record reliable transient absorption spectra this assignment remains speculative.

Thus, the magic angle transient absorption kinetics indicate that the overall population dynamics in the photoexcited $[Ru(bpy)_2(ipPhNH_2)]^{2+}$ is not affected upon integrating the complex into the block copolymer membrane. The data also reveals that the H_2O wetting the inner surface of the Ru-membrane is sufficient to protonate the photo-excited complex tethered to the inner surfaces of the membrane.

In addition to studying the excited-state population dynamics, we utilize transient absorption anisotropy to monitor orientational dynamics[47,48] of the complexes upon integration into the polymer membrane. To benchmark the transient anisotropy data of the polymer integrated complex, we first discuss the data obtained for $[Ru(bpy)_2(ipPhNH_2)]^{2+}$ in aqueous

Chemistry–A European Journal

Full Paper
doi.org/10.1002/chem.202102377

Chemistry Europe
European Chemical
Societies Publishing

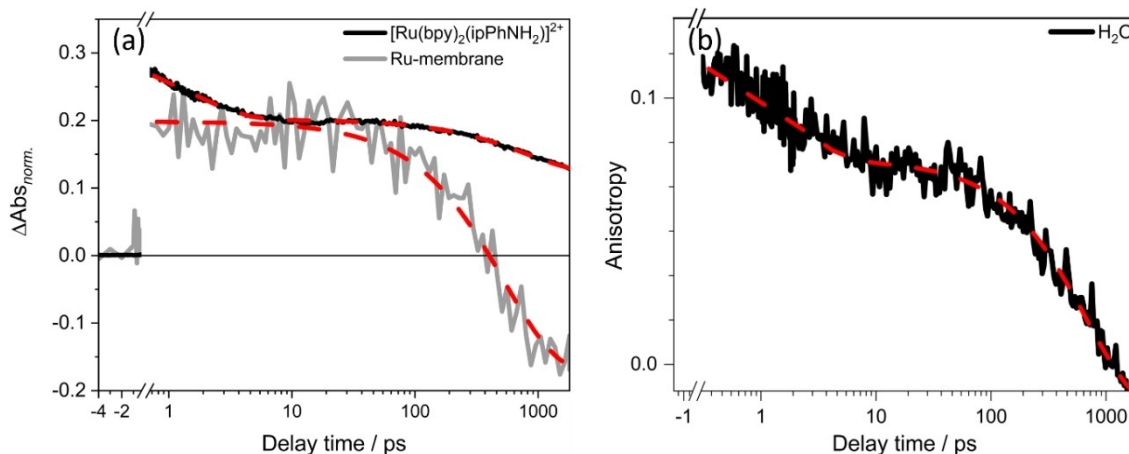**Figure 6.** (a) Transient absorption kinetics recorded under magic angle polarization, i.e., reflecting the population dynamics, of $[Ru(bpy)_2(ipPhNH_2)]^{2+}$ in H_2O and Ru-membrane. The samples were excited at 400 nm and the population dynamics was probed at 600 nm. For $[Ru(bpy)_2(ipPhNH_2)]^{2+}$ a bi-exponential fit yields time constants of 2 and 800 ps assigned to vibrational relaxation and shift in charge density from imidazole-phenanthroline to aniline portion respectively. In Ru-membrane a single exponential fit gives a time constant of 530 ps which is assigned to a shift in charge density from imidazole-phenanthroline to aniline portion of the ligand. (b) Transient absorption anisotropy kinetics of $[Ru(bpy)_2(ipPhNH_2)]^{2+}$ in H_2O ($\lambda_{pump} = 400$ nm, $\lambda_{probe} = 600$ nm). A bi-exponential fit gives time constants of 2 and 600 ps indicating that vibrational relaxation and charge transfer observed in magic angle kinetics are also responsible for change in anisotropy.

solution (Figure 6b). The initial anisotropy ($r(1ps) = 0.12$) decays to zero after about 1 ns. A fit of a bi-exponential decay to the data yields characteristic decay components of the anisotropy of 2 and 600 ps. Following previous work on transient absorption anisotropy of $[Ru(bpy)_3]^{2+}$ by Wallin et al.[42] the 2 ps component reflects the initial relaxation of the complex. Likely vibrational energy dissipation and inter-ligand hopping, i.e., localization of the excess charge density on the ip-ligand, contributes to the 2 ps component as visible in the transient anisotropy data. The slow decay of the anisotropy is due to rotational diffusion of the complexes randomizing the orientation of the transition dipole moments within the lab coordinate frame, even though the magic angle kinetics (see

above) suggest that charge localization on the protonated aniline also takes place on a similar timescale. The effect of viscosity on the rotational diffusion can be observed clearly, when considering the anisotropy of the complex in the highly viscous solvent TDE (2,2'-thiodiethanol) (Figure S6).[49,50] In this solvent a long-lived rather constant anisotropy is observed on a sub-ns timescale.

Figure 7 summarizes the transient absorption anisotropy measurements of the Ru-membrane. Due to the inherent inhomogeneity of the membrane, we recorded transient anisotropy values at difference spatial positions in the Ru-membrane. Despite the fact that the initial anisotropy, recorded at a delay time of 1 ps, varies from spot to spot, a general trend
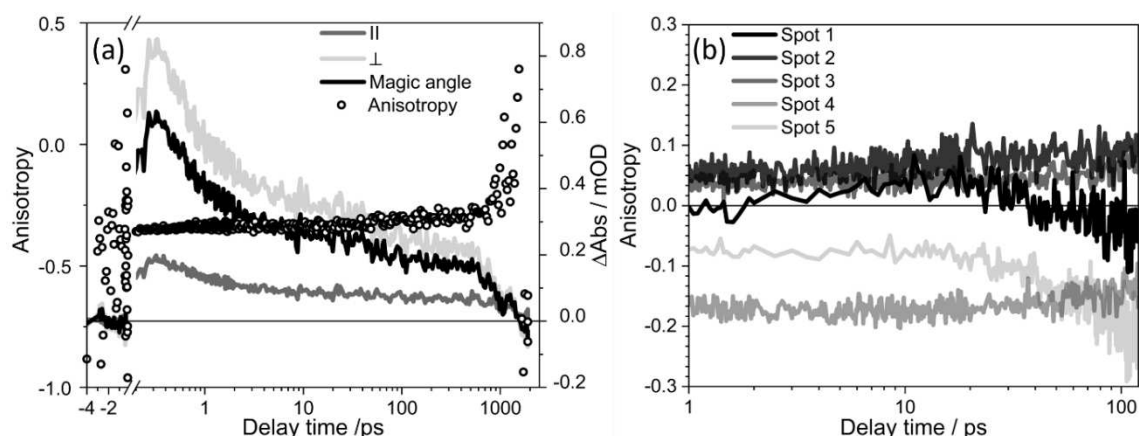

Figure 7. Transient absorption anisotropy kinetics of Ru-membranes. The kinetics were recorded at 600 nm upon optical excitation at 400 nm. (a) Comparison of the transient absorption anisotropy kinetics with the corresponding magic angle kinetics and the pump probe kinetics recorded with parallel and perpendicular pump-probe polarizations for a given spot on the Ru-membrane. (b) Comparison of transient absorption anisotropy kinetics obtained from different sample spots in Ru-membrane. The data are displayed only up to 120 ps in order to highlight the different initial anisotropies observed upon variation the position probed in the sample.

Chemistry–A European Journal

Full Paper
doi.org/10.1002/chem.202102377

Chemistry Europe
European Chemical
Societies Publishing

reflecting the integration of the complexes into the polymer membrane is apparent: $r(t)$ remains constant roughly within the first 100 ps after excitation. This reflects the fixation of each of the complexes in the polymer membrane by the covalent linkage. We would like to point out that the $r(t)$ plateau values observed range from 0.07 to 0.36. Hence, they are nearby the range of 0.4, which reflects the available anisotropy values if a single electronic transition only contributes to the signal.[51,52] Such behavior is most prominently observed in experiments concerning time-resolved fluorescence anisotropy.[53–55] This points to a complex scenario, in which more than a single electronic transition, for example, ligand-to-metal charge transfer and intra-ligand charge transfer transitions in addition to different protonation states of the complex in different local environments, contribute to the experimentally observed anisotropy as indicated by the transition dipole moments of the underlying singlet and triplet excitations (Figure S10). The scenario becomes even more complex, when considering that we might probe different amounts of aggregated chromophores or different degrees of wetting in different spots of the rather inhomogeneous membranes. However, irrespective of the spatial position at which $r(t)$ is sampled, a strong increase in anisotropy is observed at long delay times. This is entirely uncommon in systems in which rotational diffusion determines the signal on such timescales. This increase in $r(t)$ occurs in the same delay time range as the signal change of ΔAbs observed in the respective magic angle kinetics (Figures 6 and 7). As discussed above we ascribe this signal change in the magic angle kinetics charge density shift within the protonated ip-ligand. As a result, additional electronic states become available to be probed in the transient anisotropy experiment. Even though an in-depth description of the individual states contributing to this abrupt change in anisotropy at long delay lines is out of the focus of this report, our results highlight the rigidity in the molecular environment in polymer membranes.

Our studies indicate a severe restriction of molecular reorientation upon incorporation of $[Ru(bpy)_2(ipPhNH_2)]^{2+}$ into the block copolymer membranes. The rigidly linked chromophores show an increased emission quantum yield, which amounts to 9.2% compared to $[Ru(bpy)_2(ipPhNH_2)]^{2+}$ in solution, where an estimated Φ_{em} of 3.5% is recorded due to an increase in non-radiative deactivation channels via collisions and rotations (Figure S7). While the overall excited-state relaxation seems only marginally effected, the restricted molecular motion might impact the collision induced inter-actions between the photoactive complexes and other molecular components of photocatalytic systems, for example, sacrificial electron donors or catalysts. Hence, it appears worthwhile to study different molecular linkages between the photoactive metal center and the polymer backbone in the future, which might allow for more structural mobility of the chromophore after integration into the membrane.[56]

Conclusion

We prepared nanoporous block copolymer membranes and functionalized them covalently with a [Ru]-based photosensitizer. This led to a highly increased loading in comparison to electrostatically attached photosensitizers[9] and lays the foundation for further research on this kind of membranes for photocatalytic applications. We investigated the orientational diffusion of a Ru(II) chromophore when integrated into a porous block copolymer membrane by ultrafast transient absorption anisotropy. Even though Ru-membrane integration does not alter the overall excited-state relaxation (in terms of population dynamics) significantly, we observe that a very heterogeneous ensemble contributes to the spectroscopic signatures obtained from the Ru-membranes, which is due to the formation of aggregates of complexes and different protonation stages of the complex in the membrane. Nonetheless, irrespective of the position within the Ru-membrane, which we probe, the transient absorption anisotropy, indicating the orientation of the probed transition dipole moment, remains constant for several 100 ps after excitation. This indicates that polymer integration of the complex significantly hinders its local mobility. This might be a relevant factor to consider, when optimizing such porous polymer membranes towards improved photocatalytic activity, as photocatalysis by membrane integrated molecular components requires multiple intermolecular collisions, for example, between photocenter and sacrificial agents and catalysts, to proceed.

Experimental Section

Block copolymer synthesis: All chemicals and analytical grade solvents were purchased from Sigma-Aldrich Chemie GmbH (Munich, Germany). BlocBuilderMA was kindly donated by Sylvain Bourrigaud from Arkema (Colombes, France) and used as received. The $[Ru(bpy)_2(ipPhNH_2)]Cl_2$ photosensitizer was prepared as reported previously.[18]

For the synthesis of the poly(styrene-co-isoprene) block the initiator Blocbuilder MA (130 mg) was dissolved in a mixture of 72.2 mL styrene ([M]/[I] = 1800) and 8.2 mL isoprene ([M]/[I] = 550). The oxygen was removed from the reaction mixture by three freeze-pump-thaw cycles and the reaction vessel was subsequently filled with argon. The reaction mixture was heated at 110 °C for 25 h. Subsequently the mixture was cooled down in liquid nitrogen. The resulting copolymer was precipitated twice in cold methanol ($M_n = 37,800$ g mol^{-1}, Đ = 1.25).

In the second step, 0.38 g of the macroinitiator poly(styrene-co-isoprene) ($M_n = 37,800$ g mol^{-1}) was dissolved in 4 mL anisole and the monomers TEGA (0.43 mL, [M]/[I] = 200) and VBCL (0.75 mL, [M]/[I] = 450) were added. The reaction mixture was subsequently degassed by three freeze-pump thaw-cycles. Afterwards the reaction vessel was filled with argon and heated at 110 °C for 22.5 h. VBCI was purified before use by distillation and the stabilizer of TEGA was removed by passing through a short column of basic alumina. After the polymerization, the reaction mixture was cooled down to room temperature and precipitated three times in hexane ($M_n = 74,600$ g mol^{-1}, Đ = 1.37).

Membrane fabrication: Membranes were prepared via the NIPS process as described previously: films were cast onto glass

Chemistry–A European Journal

Full Paper
doi.org/10.1002/chem.202102377

Chemistry Europe
European Chemical
Societies Publishing

substrates from 15 wt% block copolymer solution in THF/DMF (70/30 wt%) solvent mixtures using a 200 mm gate height doctor blade. The film casting was carried out in a climate chamber from PlasLabs (US) at controlled humidity (50%) and temperature (22°C). After casting, the membrane was exposed to air for 15 s (so called "open time"), followed by fast immersion into a bath of deionized water, in which the block copolymer precipitates and self-assembles to form the porous membranes. After the membranes lifted off from the glass substrates the membranes were stored in deionized water. The functionalization of the membranes was conducted in 30 mL of a solvent mixture of water and methanol (ratio 2:1). For every unit of VBCl in the block copolymer a unit of **[Ru-(bpy)₂(ipPhNH₂)]Cl₂** was added to the solution and 3 units of triethylamine were added for the deprotonation of the ipPhNH₂ ligand. This reaction mixture was stirred at 50°C for 24 h. Subsequently the Ru-membrane was washed three times with deionized water (3×30 mL) and stored in deionized water.

Sample preparation for spectroscopy: To prevent Ru-membrane from turning brittle, all experiments were conducted with Ru-membrane soaked in H_2O. This was followed by firmly compressing the membrane between two glass slides.

Instrumentation

Nuclear magnetic resonance spectroscopy (NMR): ^{1}H NMR spectra were measured on a 300 MHz Bruker AVANCE spectrometer using $CDCl_3$, as deuterated solvent at a temperature of 298 K. The solvent residual peak $CDCl_3$ was used as standard.

Size exclusion chromatography (SEC): SEC measurements in THF were performed on an Agilent system equipped with a G1310 A pump, a G1362 A refractive index detector, and both a PSS Gram30 and a PSS Gram1000 column in series. THF was applied as eluent at 1 mL min⁻¹ flow rate and the column oven was set to 40°C. For calibration polystyrene standards were used.

Scanning electron microscopy (SEM): SEM was performed on a Zeiss (Oberkochen, Germany) (LEO) 1530 Gemini FESEM operating at 5 to 10 kV using an InLens detector. Previously, the samples were coated with gold (~5 nm) using a SCD005 sputtering device BAL-TEC (Balzers, Liechtenstein).

Thermogravimetric analysis (TGA): TGA was performed on a Perkin-Elmer-TGA 8000 instrument under airflow (20 mL min⁻¹) at a heating rate of 10°C min⁻¹.

X-ray photoelectron spectroscopy (XPS): XPS was performed using a UHV Multiprobe system (Scienta Omicron, Germany) with a monochromatic X-ray source (Al K_α) and an electron analyzer (Argus CU) with 0.6 eV energy resolution. Charge compensation during data acquisition was realized by an electron flood gun (NEK 150SC, Staib, Germany) at 6 eV and 50 μA. The background was subtracted, and spectra were calibrated using the C 1s peak (284.6 eV) before undergoing fitting using Voigt functions (30:70).

Steady-state spectroscopy: Steady state absorption of **[Ru-(bpy)₂(ipPhNH₂)]²⁺** in H_2O under air equilibrated conditions in a 1 cm quartz cell was recorded with JASCO V-760 spectrophotometer. For Ru-membrane, the membrane was gently dried with N_2 flow to remove excess H_2O. The Ru-membrane was then sandwiched between two glass slides and the absorption recorded in reflectance mode in an Ulbricht sphere. The reference used herein was the polymer membrane without the Ru complex sandwiched between two glass slides. Steady state emission spectra were recorded in Fluorolog (HORIBA) spectrophotometer. For **[Ru-(bpy)₂(ipPhNH₂)]²⁺** in H_2O an OD of 0.05 was maintained under air equilibrated condition in a 1 cm quartz cuvette. In Ru-membrane

an exact similar sample preparation procedure like in the UV-vis absorption experiment was adopted. Emission quantum yield ($\Phi_{em.}$) for Ru-membrane was measured using an integrated sphere with a step size and dwell time of 1 nm and 0.5 s respectively. The quantum yield of **[Ru(bpy)₂(ipPhNH₂)]²⁺** in water was determined by using a $[Ru(bpy)_3](PF_6)_2$ salt as a standard reference with $\Phi_{em.} = 4\%$.[19] For rR spectroscopy a laser beam of 405 nm, generated from a diode laser(TOPMODE-405-HP, TOPTICA) with an output power of 5 mW was focused on a 1 mm quartz cuvette containing **[Ru-(bpy)₂(ipPhNH₂)]²⁺** maintained at an OD of 0.2 at the excitation wavelength. The scattered pump beam was blocked using a filter and the rR scattered light was collected and directed to a spectrophotometer (ISOPLANE 160, Princeton Instruments) with a grating of 2400 groves per 1 mm. The signal was detected using a thermoelectrically cooled CCD (EXCELON, Princeton Instruments). rR signals could not be detected above 2000 cm⁻¹ due to strong phosphorescence from the sample. Background correction of the signal was done following established protocols on peak detection by continuous wavelet transform (CWT), peak width estimation by signal to noise ratio (SNR) enhancing derivative calculation and back ground fitting using penalized least squares with binary masks.[20]

Time resolved spectroscopy: The setup for white light fs-TA spectroscopy has been described elsewhere.[21,22] For fs-TA anisotropy measurements the probe generated in a NOPA (TOPAS white, LightConversion) was split into two beams, one part of the probe was set at a polarization parallel to the pump beam while the other beam had its polarization flipped by 90° w.r.t the pump beam. These three beams were then made incident on the sample spot. The probe beams were directed to their respective photodiodes (Pascher Instruments AB) and the signal recorded. The power of the pump beam was attenuated to 8 μW to avoid degradation of Ru-membrane. The anisotropy $r(t)$ and the magic angle signal $I_{54.7°}(t)$ were calculated from the transient absorption signals recorded with parallel and perpendicular polarization. Time resolved ns emission was recorded using a 10 Hz NdYAG laser coupled as excitation source to an optical parametric oscillator (OPO) generating 410 nm pump beam. Full details about the experimental setup can be found in Ref. [23].

Conflict of Interest

The authors declare no conflict of interest.

[1] I. Romanenko, M. Lechner, F. Wendler, C. Hörenz, C. Streb, F. H. Schacher, *J. Mater. Chem. A* **2017**, *5*, 15789–15796.

[2] J. Hahn, J. I. Clodt, V. Filiz, V. Abetz, *RSC Adv.* **2014**, *4*, 10252–10260.

[3] R. John, K. Pal, J. S. Jayan, S. Appukuttan, *J. Mol. Struct.* **2021**, *1231*, 129926.

[4] L. C. Lopez, M. G. Buonomenna, E. Fontananova, E. Drioli, P. Favia, R. d'Agostino, *Plasma Processes Polym.* **2007**, *4*, 326–333.

[5] V. Abetz, T. Brinkmann, M. Dijkstra, K. Ebert, D. Fritsch, K. Ohlrogge, D. Paul, K. Peinemann, S. Pereira-Nunes, N. Scharnagl, *Adv. Eng. Mater.* **2006**, *8*, 328–358.

[6] W. A. Phillip, R. M. Dorin, J. Werner, E. M. V. Hoek, U. Wiesner, M. Elimelech, *Nano Lett.* **2011**, *11*, 2892–2900.

[7] V. Abetz, *Macromol. Rapid Commun.* **2015**, *36*, 10–22.

[8] M. Bonchio, M. Carraro, G. Scorrano, E. Fontananova, E. Drioli, *Adv. Synth. Catal.* **2003**, *345*, 1119–1126.

[9] I. Romanenko, A. Rajagopal, C. Neumann, A. Turchanin, C. Streb, F. H. Schacher, *J. Mater. Chem. A* **2020**, *8*, 6238–6244.

[10] K. Peter, M. Thelakkat, *Macromolecules* **2003**, *36*, 1779–1785.

[11] V. Marin, E. Holder, U. S. Schubert, *J. Polym. Sci. Part A* **2004**, *42*, 374–385.

[12] V. Marin, E. Holder, R. Hoogenboom, U. S. Schubert, *Chem. Soc. Rev.* **2007**, *36*, 618–635.

[13] L. Zhang, J. M. Cole, *J. Mater. Chem. A* **2017**, *5*, 19541–19559.

[14] M. Pastore, F. De Angelis, I. Cnr, *ACS Nano* **2010**, *4*, 556–562.

[15] N. Robertson, *Angew. Chem. Int. Ed.* **2006**, *45*, 2338–2345; *Angew. Chem.* **2006**, *118*, 2398–2405.

[16] N. J. Cherepy, G. P. Smestad, M. Grätzel, J. Z. Zhang, *J. Phys. Chem. B* **1997**, *101*, 9342–9351.

[17] A. Listorti, B. O'Regan, J. R. Durrant, *Chem. Mater.* **2011**, *23*, 3381–3399.

[18] A. Stumper, M. Lämmle, A. K. Mengele, D. Sorsche, S. Rau, *Eur. J. Inorg. Chem.* **2018**, *2018*, 586–596.

[19] K. Suzuki, A. Kobayashi, S. Kaneko, K. Takehira, T. Yoshihara, H. Ishida, Y. Shiina, S. Oishi, S. Tobita, *Phys. Chem. Chem. Phys.* **2009**, *11*, 9850–9860.

[20] A. Baiardi, C. Latouche, J. Bloino, V. Barone, *Dalton Trans.* **2014**, *43*, 17610–17614.

[21] M. Karnahl, C. Kuhnt, F. Ma, A. Yartsev, M. Schmitt, B. Dietzek, S. Rau, J. Popp, *ChemPhysChem* **2011**, *12*, 2101–2109.

[22] R. Siebert, D. Akimov, M. Schmitt, A. Winter, U. S. Schubert, B. Dietzek, J. Popp, *ChemPhysChem* **2009**, *10*, 910–919.

[23] M. Stephenson, C. Reichardt, M. Pinto, M. Wa, T. Sainuddin, G. Shi, H. Yin, S. Monro, E. Sampson, B. Dietzek, S. A. Mcfarland, *J. Phys. Chem. A* **2014**, *118*, 10507–10521.

[24] F. Schacher, T. Rudolph, F. Wieberger, M. Ulbricht, A. H. E. Müller, *ACS Appl. Mater. Interfaces* **2009**, *1*, 1492–1503.

[25] J. K. McCusker, *Acc. Chem. Res.* **2003**, *36*, 876–887.

[26] N. H. Damrauer, G. Cerullo, A. Yeh, T. R. Boussie, C. V. Shank, J. K. McCusker, *Sci. J.* **1997**, *275*, 54–57.

[27] M. Wächtler, J. Guthmuller, L. González, B. Dietzek, *Coord. Chem. Rev.* **2012**, *256*, 1479–1508.

[28] C. W. Chang, C. K. Chou, I. J. Chang, Y. P. Lee, E. W. G. Diau, *J. Phys. Chem. C* **2007**, *111*, 13288–13296.

[29] A. Chettri, J. A. Roque, K. R. A. Schneider, H. D. Cole, C. G. Cameron, S. A. McFarland, B. Dietzek, *ChemPhotoChem* **2021**, *5*, 1–6.

[30] J. Van Houten, R. J. Watts, *J. Am. Chem. Soc.* **1976**, *98*, 4853–4858.

[31] Y. C. Lu, E. W. G. Diau, H. Rau, *J. Phys. Chem. A* **2005**, *109*, 2090–2099.

[32] M. Devenney, L. A. Worl, S. Gould, A. Guadalupe, B. Patrick Sullivan, J. V. Caspar, R. L. Leasure, J. R. Gardner, T. J. Meyer, *J. Phys. Chem. A* **1997**, *101*, 4535–4540.

[33] S. Bernhard, J. A. Barron, P. L. Houston, D. Abrun, J. L. Ruglovksy, X. Gao, G. G. Malliaras, *J. Am. Chem. Soc.* **2002**, *124*, 13624–13628.

[34] K. W. Lee, J. D. Slinker, A. A. Gorodetsky, S. Flores-Torres, H. D. Abruña, P. L. Houston, G. G. Malliaras, *Phys. Chem. Chem. Phys.* **2003**, *5*, 2706–2709.

[35] G. Zou, K. Fang, P. He, W. Lu, *Thin Solid Films* **2004**, *457*, 365–371.

[36] K. Peuntinger, T. D. Pilz, R. Staehle, M. Schaub, S. Kaufhold, L. Petermann, M. Wunderlin, H. Görls, F. W. Heinemann, J. Li, T. Drewello, J. G. Vos, D. M. Guldi, S. Rau, *Dalton Trans.* **2014**, *43*, 13683–13695.

[37] S. Campagna, F. Puntoriero, F. Nastasi, G. Bergamini, V. Balzani, *Top. Curr. Chem.* **2007**, *280*, 117–214.

[38] A. Cannizzo, F. van Mourik, W. Gawelda, G. Zgrablic, C. Bressler, M. Chergui, *Angew. Chem.* **2006**, *118*, 3246–3248; *Angew. Chem. Int. Ed.* **2006**, *45*, 3174–3176.

[39] C. W. Stark, W. J. Schreier, J. Lucon, E. Edwards, T. Douglas, B. Kohler, *J. Phys. Chem. A* **2015**, *119*, 4813–4824.

[40] W. Henry, C. G. Coates, C. Brady, K. L. Ronayne, P. Matousek, M. Towrie, S. W. Botchway, A. W. Parker, J. G. Vos, W. R. Browne, J. J. McGarvey, *J. Phys. Chem. A* **2008**, *112*, 1073–1074.

[41] A. El Nahhas, A. Cannizzo, F. Van Mourik, A. M. Blanco-Rodríguez, S. Záliš, A. Vlček, M. Chergui, *J. Phys. Chem. A* **2010**, *114*, 6361–6369.

[42] S. Wallin, J. Davidsson, J. Modin, L. Hammarström, *J. Phys. Chem. A* **2005**, *109*, 4697–4704.

[43] B. Jing, T. Wu, C. Tian, M. Zhang, T. Shen, *Bull. Chem. Soc. Jpn.* **2000**, *73*, 1749–1755.

[44] M. J. Han, L. H. Gao, Y. Y. Lü, K. Z. Wang, *J. Phys. Chem. B* **2006**, *110*, 2364–2371.

[45] A. O. Eseola, O. Adepitan, H. Görls, W. Plass, *New J. Chem.* **2012**, *36*, 891–902.

[46] H. Yin, F. Cheng, Z. Liu, C. He, Y. Yang, K. Wang, *J. Coord. Chem.* **2019**, *72*, 2957–2967.

[47] P. Hazra, D. Chakrabarty, A. Chakraborty, N. Sarkar, *Biochem. Biophys. Res. Commun.* **2004**, *314*, 543–549.

[48] J. R. Unruh, G. Gokulrangan, G. H. Lushington, C. K. Johnson, G. S. Wilson, *Biophys. J.* **2005**, *88*, 3455–3465.

[49] F. L. G. Flecha, V. Levi, *Biochem. Mol. Biol. Educ.* **2003**, *31*, 319–322.

[50] B. W. van der Meer, R. P. van Hoeven, W. J. van Blitterswijk, *BBA-Biomembranes* **1986**, *854*, 38–44.

[51] G. B. Shaw, C. L. Brown, J. M. Papanikolas, *J. Phys. Chem. A* **2002**, *106*, 1483–1495.

[52] D. M. Jonas, M. J. Lang, Y. Nagasawa, T. Joo, G. R. Fleming, *J. Phys. Chem.* **1996**, *100*, 12660–12673.

[53] J. R. Lakowicz, G. Freshwater, G. Weber, *Biophys. J.* **1980**, *32*, 591–601.

[54] J. M. Beechem, L. Brand, *Annu. Rev. Biochem.* **1985**, *54*, 43–71.

[55] A. M. Breul, J. Schäfer, G. M. Pavlov, A. Teichler, S. Höppener, C. Weber, J. Nowotny, L. Blankenburg, J. Popp, M. D. Hager, B. Dietzek, U. S. Schubert, *J. Polym. Sci. Part A* **2012**, *50*, 3192–3205.

[56] F. N. Castellano, T. A. Heimer, M. T. Tandhasetti, G. J. Meyer, *Chem. Mater.* **1994**, *6*, 1041–1048.